





## Experimental observation of coherent-perfect-absorber and laser points in anti-PT symmetry

Minye Yang <sup>1,2,\*</sup> Qi Zhong,<sup>3,\*</sup> Zhilu Ye <sup>1,2</sup> Şahin K. Özdemir <sup>3,4</sup> Mohamed Farhat,<sup>5</sup>  
Ramy El-Ganainy,<sup>6,7</sup> and Pai-Yen Chen <sup>2,†</sup>

<sup>1</sup>State Key Laboratory for Manufacturing Systems Engineering, School of Electronic Science and Engineering, Xi'an Jiaotong University, Xi'an 710049, Shaanxi, China

<sup>2</sup>Department of Electrical and Computer Engineering, University of Illinois at Chicago, Chicago, Illinois 60607, United States

<sup>3</sup>Department of Engineering Science and Mechanics, The Pennsylvania State University, University Park, Pennsylvania 16802, USA

<sup>4</sup>Materials Research Institute, Pennsylvania State University, University Park, Pennsylvania 16802, USA

<sup>5</sup>Computer, Electrical, and Mathematical Science and Engineering Division, King Abdullah University of Science and Technology, Thuwal 23955-6900, Saudi Arabia

<sup>6</sup>Department of Physics, Michigan Technological University, Houghton, Michigan 49931, USA

<sup>7</sup>Henes Center for Quantum Phenomena, Michigan Technological University, Houghton, Michigan 49931, USA



(Received 11 January 2024; revised 13 June 2024; accepted 9 August 2024; published 3 September 2024)

The coexistence of coherent perfect absorber and laser or amplifier (CPAL) point is a peculiar spectral singularity associated with the scattering matrices of non-Hermitian systems. While the potential of CPAL systems for sensing application has been highlighted recently, the extreme sensitivity of parity-time (PT)-symmetric CPAL devices to the input signal deviations has so far impeded their practical utilization. Here we explore a strategy for implementing CPAL circuits by exploiting another type of non-Hermitian symmetry, namely anti-PT (APT) symmetry. We demonstrate that the condition for building CPAL in our proposed APT-symmetric electronic circuits additionally requires parity symmetry, which simplifies the circuit design and implementation. Additionally, we show that this newly proposed structure is 1.85 times more robust compared to previous CPAL devices studied in the literature.

DOI: [10.1103/PhysRevA.110.033504](https://doi.org/10.1103/PhysRevA.110.033504)

### I. INTRODUCTION

The notion of symmetry is fundamental to modern physics. In Hermitian systems, which include standard quantum mechanical problems and optical structures without gain or loss, various symmetry transformations—such as translation, rotational, and parity symmetries—play a crucial role in understanding and classifying the solutions of underlying equations of motion, such as the Schrödinger equation or Maxwell's equations. Meanwhile, in recent decades, it was observed how symmetries have significant implications in non-Hermitian systems, especially with the discovery of parity-time (PT) symmetry [1,2]. Among them, an important and counterintuitive outcome of PT symmetry is that the non-Hermitian Hamiltonian can have real eigenvalues [1], like its Hermitian counterpart.

While non-Hermitian notations are useful for describing any open systems, optical platforms particularly attracted considerable attention, mainly due to their versatility and potential applications [3–5]. The unique features of non-Hermitian photonic systems are enabled by the peculiar spectral characteristics associated with their underlying non-Hermitian Hamiltonians  $H$  and scattering matrices  $S$ . The first

describes the evolution of optical fields within the optical system while the second establishes the relationship between the input and output fields. Both non-Hermitian Hamiltonians and scattering matrices feature non-Hermitian singularities known as exceptional points (EPs), at which both the eigenvalues and the corresponding eigenmodes coalesce, signaling the breakdown of typical perturbation analysis and giving rise to eigenvalue bifurcation and an enhanced response to perturbations [5–7]. Other important spectral points include the zeros and poles of the scattering matrix [8], defined by its eigenvalues. When a zero of  $S$  occurs on the real axis at  $\omega$  in the complex frequency plane, the response of all output channels vanishes under a particular superposition of inputs (oscillating as  $e^{-i\omega t}$ ) specified by the associated eigenmodes, thereby acting as a coherent perfect absorber (CPA) [9–16]. However, the poles of scattering matrices act as self-oscillating devices, typically functioning as lasers in optical systems. A special scenario involving the coexistence of CPA and laser can occur when a pair of zero and pole coincide at the real frequency, which was theoretically introduced in PT-symmetric optical systems [17] and later verified experimentally [18].

Soon after introducing the notion of PT symmetry in optical systems, where the above works were mainly developed, it was realized that the concept could be extended to other platforms such as electronics [19,20] and acoustics [21]. The first is of particular interest given the abundance of electronic devices and technologies that infiltrate every aspect of our daily

\*These authors contributed equally.

†Contact author: pychen@uic.edu

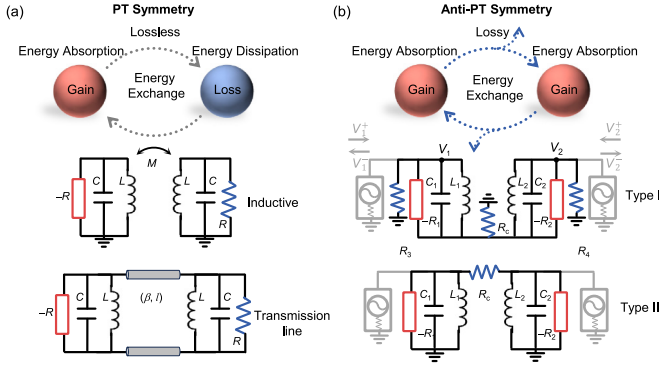


FIG. 1. (a) A diagram of a standard PT-symmetric system comprising a pair of gain and loss components, and a lossless energy interaction between them. The lower panel of (a) depicts two typical realizations in electronics. (b) A schematic illustration of an APT-symmetric system consisting of two gain components with lossy energy interaction. The lower panel of (b) illustrates two types of electronic APT circuits. The gray part illustrates the ports for measuring the scattering properties.

lives. In this regard, recent works on PT-symmetric electronic sensors [22–25] and encryption schemes [26] demonstrated the great potential of non-Hermitian electronic systems in real life applications. A particular class of phenomenon in non-Hermitian electronic circuits that can be of utility in several applications is that associated with the aforementioned CPA and CPAL points, which was demonstrated in PT-symmetric circuits [19] and shown to have promising potential for sensing [27,28] and encryption [29] applications. Unfortunately, standard implementations of CPAL based on PT symmetry suffered from several drawbacks. First, achieving PT symmetry requires the coupling of two oscillators with a delicate balance between the net gain or loss values and their coupling coefficients [Fig. 1(a)], which in turn imposed stringent conditions on the fabrication tolerance. Second, the system was also sensitive to imperfections and deviations in the input signal. It was demonstrated that a small perturbation of the input signal will result in nonzero output, which, for practical values of noise, was still relatively large compared to the optimal situation. It is thus beneficial to engineer new systems that exhibit CPAL points with high feasibility and better robustness against input variations when tuned to the CPA operation regime.

Here we propose and demonstrate an alternative implementation of CPAL in electronic circuits that rely on anti-parity-time (APT) symmetry [30–34]. A pair of coupled RLC circuits respecting APT symmetry by implementing the dissipative (imaginary) coupling with a resistor was demonstrated in Ref. [32] and illustrated as type II in Fig. 1(b). In this paper, we propose a configuration of APT-symmetric coupled RLC circuits as shown as type I in Fig. 1(b). Based on the temporal coupled-mode theory [35] analysis, the APT symmetry (in terms of the Hamiltonian) requires that the RLC tanks on the left and right sides in these two types of circuits should have identical resistances and capacitances, but can have different values of inductances, which causes frequency detuning. However, the analysis of eigenvalues of scattering matrices shows that CPAL can occur in both under

specific conditions, one of which is that the inductors of both oscillators should be identical. This additional condition for CPAL makes two configurations adhere to parity symmetry, in addition to APT symmetry. This, in turn, facilitates the system design and fabrication and demonstrates the more robust operation of the input signal.

## II. CPA-LASER IN ANTI-PARITY-TIME SYMMETRY

We consider the non-Hermitian circuit designs, types I and II, as illustrated in Fig. 1(b). The dynamics of these circuits, in terms of the voltage  $V_{1,2}$  on left and right tanks, can be expressed in the Liouvillian formalism by applying Kirchhoff's laws, see Appendix A for details. The APT symmetry condition of the type-II circuit is provided in Ref. [32], within the framework of temporal coupled-mode theory [35], and that is  $C_1 = C_2 = C$ ,  $R_1 = R_2 = R$  (the negative resistance  $-R_{1,2}$  in Fig. 1 represent gain). Here we adopt the same approach and derive the effective Hamiltonian for the type-I circuit

$$H_I = \begin{bmatrix} \Delta\omega + ig_1 & ik_1 \\ ik_2 & -\Delta\omega + ig_2 \end{bmatrix}, \quad (1)$$

where  $\Delta\omega = \omega_1 - \omega_2$  with  $\omega_{1,2} = \sqrt{L_{1,2}C_{1,2}}$ . Here the gain (or loss)  $g_{1,2}$  and the coupling  $k_{1,2}$  rely on the values of  $R_n$ ,  $L_n$ , and  $C_n$  in Fig. 1(b), and are given in Appendix A. The APT symmetry requires  $H$  anticommutes with parity operator ( $P$ ) and time-reversal operator ( $T$ ), i.e.,  $\{H, PT\} \equiv HPT + PTH = 0$ , leading to  $k_1 = k_2$  and  $g_1 = g_2$ , and therefore,  $C_1 = C_2 = C$ ,  $R_1 = R_2 = R$ , and  $R_3 = R_4$  (see Appendix A for details). In both configurations, the values of  $L_{1,2}$  do not need to be equal. Their ratio is denoted by  $s \equiv L_1/L_2$  and can be utilized to tune the frequency detuning  $\Delta\omega$ , thereby adjusting the system to an EP or causing the eigenvalues to split into the real or imaginary parts. In the following, we will show that to achieve the CPAL in both APT-symmetric circuits,  $s$  must equal unity.

To investigate the possibility of CPAL points in these APT circuits, we connect the isolated circuits into an input-output channel as shown in Fig. 1(b) and their corresponding scattering matrices  $S$  connect the output and input fields, i.e.,  $|V_{\text{out}}\rangle = S_{I,II} |V_{\text{in}}\rangle$  where  $|V_{\text{in}}\rangle = (V_1^+, V_2^+)^T$  and  $|V_{\text{out}}\rangle = (V_1^-, V_2^-)^T$ . The closed-form solution for  $S$  can be obtained either from the corresponding Hamiltonian matrices or by analyzing their admittance matrices, as detailed in Appendix B. The CPAL condition necessitates that one eigenvalue of  $S$  equals 0 and another equals infinity at a real input frequency  $\omega$ , leading to the important result  $s = 1$ , see Appendix B for explicit derivation. An immediate consequence of this condition is that the frequency detuning  $\Delta\omega = 0$  in Eq. (1), and the entire structure is symmetric around the center line, representing parity symmetry. This parity symmetry is also evident from the Hamiltonian of both circuits in the form of  $H = i \begin{bmatrix} g & k \\ k & g \end{bmatrix}$ , satisfying  $[P, H] \equiv PH - HP = 0$ . This additional parity symmetry, in turn, facilitates the system design and fabrication which will be discussed later. Note here that the  $H$  for  $\Delta\omega = 0$  has no EP but a Weyl (diabolic) point at  $k = 0$  as its eigenvectors are still independent while the eigenvalues degenerate.

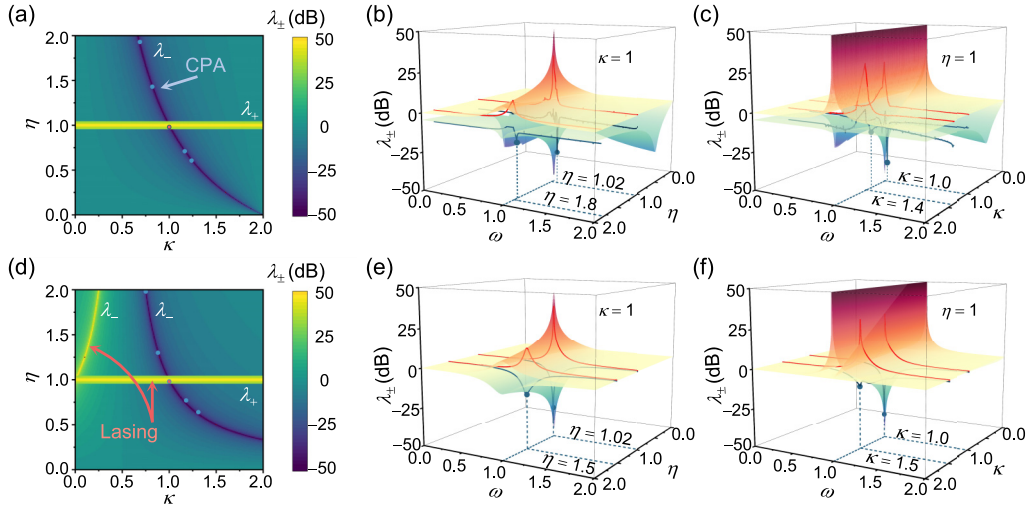


FIG. 2. (a) Color map of the eigenvalues  $\lambda_{\pm}$  of the scattering matrix of type I APT-symmetric system as functions of  $\eta$  and  $\kappa$  at operating frequency  $\omega = 1$ . The eigenmode associated with  $\lambda_{-}$  can be a CPA mode when  $\eta = 1/(2\kappa - 1)$  or a lasing mode when  $\eta = 1/(1 - 2\kappa)$ . The eigenmode associated with  $\lambda_{+}$  is a lasing mode when  $\eta = 1$  ( $\lambda_{+}$  is plotted around this value). The intersection of  $\lambda_{-} = 0$  and  $\lambda_{+} = \infty$  is the CPAL condition. Spectral behavior of eigenvalues of scattering matrices as functions of  $\eta$  in (b) and  $\kappa$  in (c) for type-I APT-symmetric system. (d)–(f) are similar to (a)–(c), but for the type-II APT-symmetric system. The condition for  $\lambda_{-} = 0$  is  $\eta = 2/\kappa - 1$ . Here, for all plots,  $\gamma = 0.2$  is selected to comply with our experiments. Data points and solid lines are experimental results.

To verify the CPAL phenomenon by two APT systems, the eigenvalues associated with the scattering matrices corresponding to two types of APT circuits,  $\lambda_{I,II}$ , are exploited under  $s = 1$ , which can be expressed as

$$\begin{aligned}\lambda_{I+} &= 1 - \frac{2\gamma\eta\omega}{\gamma\omega(\eta - 1) + i(\omega^2 - 1)}, \\ \lambda_{I-} &= 1 + \frac{2\gamma\omega - 2i(\omega^2 - 1)}{\gamma\omega(\eta - 1 - 2\eta\kappa) + i(1 + 2\eta\kappa)(\omega^2 - 1)}, \\ \lambda_{II+} &= -1 + \frac{2\gamma\eta\omega}{\gamma\omega(\eta - 1) + i(\omega^2 - 1)}, \\ \lambda_{II-} &= 1 - \frac{2\gamma\eta\omega}{\gamma\omega(\eta - 1 + 2\kappa^{-1}) + i(\omega^2 - 1)},\end{aligned}\quad (2)$$

where  $\gamma = \sqrt{L/C}/R$  is the quality factor of circuits and  $\kappa = R_c/R$  is the resistive coupling rate between two oscillators. In addition,  $\eta = R/Z_0$  is the gain level of this non-Hermitian system where  $Z_0$  is the port impedance. In the type-I circuit,  $Z_0$  is in parallel to  $R_{3,4}$  and therefore we can equivalently make  $R_3 = R_4 = Z_0$ . Here the input frequency  $\omega$  is normalized with respect to resonance frequency  $\omega_0 = 1/\sqrt{LC}$ . The CPAL condition requires that  $\lambda_{+} = \infty$  and  $\lambda_{-} = 0$  in Eq. (2), or vice versa, leading to  $\kappa$ ,  $\eta$ , and  $\omega$  being equal to 1 while  $\gamma$  is arbitrary. Figures 2(a) and 2(d) present contour plots for the eigenvalues demonstrating the various operating regimes. The intersection between the CPA and lasing lines represents the CPAL point. Figures 2(b), 2(c), 2(e), and 2(f) numerically present the spectral behavior of eigenvalues of both APT systems as functions of  $\eta$  and  $\kappa$ , validating our analytical results of the occurrence of CPAL effect.

At the exact CPAL point, all four elements in  $S_{I,II}$  are infinity. To analyze the properties of scattering matrices, we let the systems operating just below the lasing threshold as an amplifier, i.e.,  $\eta$  approaches 1. Then, the CPA and lasing

(actually amplifying point just below the lasing threshold) can be probed experimentally by using input signals that coincide with the eigenvectors corresponding to the CPA and lasing eigenvalues. At  $\omega = \kappa = 1$ ,  $S_{I,II}$  can be expressed as

$$\begin{aligned}S_I &= \frac{-1}{\eta^2 - 1} \begin{bmatrix} \eta^2 + 1 & -2\eta \\ -2\eta & \eta^2 + 1 \end{bmatrix} \xrightarrow{\eta \rightarrow 1} -A \begin{bmatrix} 1 & -1 \\ -1 & 1 \end{bmatrix}, \\ S_{II} &= \frac{1}{\eta^2 - 1} \begin{bmatrix} \eta^2 + 1 & 2\eta \\ 2\eta & \eta^2 + 1 \end{bmatrix} \xrightarrow{\eta \rightarrow 1} A \begin{bmatrix} 1 & 1 \\ 1 & 1 \end{bmatrix},\end{aligned}\quad (3)$$

where  $A = 2(\eta - 1)^{-1}$  and approaches infinity as  $\eta \rightarrow 1$ . The absolute values of eigenvalues are  $2A$  (amplifier) and  $(2A)^{-1}$  (CPA) for both  $S_{I,II}$ , corresponding to the magnitudes of the peaks and dips in the spectrum (as in Fig. 3). The eigenvectors of  $S_{I,II}$  for amplifier are  $|V_{I+}\rangle = (1, -1)^T$  and  $|V_{II+}\rangle = (1, 1)^T$ , while for CPA are  $|V_{I-}\rangle = (1, 1)^T$  and  $|V_{II-}\rangle = (1, -1)^T$ . As a side note, we remark that these eigenvectors remain the same even when  $\omega \neq 1$ .

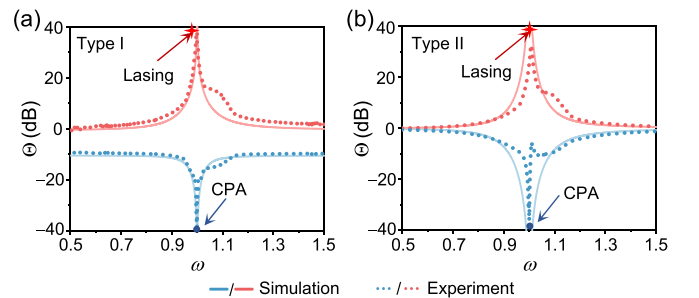


FIG. 3. Measured (dotted lines) and simulation (solid lines) of output coefficients of the (a) type I and (b) type II APT structures. Red and blue colors represent the lasing and CPA operation of the system.

The above analysis can also be understood by inspecting the expression for the total output energy associated with the system when normalized by the total input energy, i.e.,  $\Theta = \frac{|V_1^-|^2 + |V_2^-|^2}{|V_1^+|^2 + |V_2^+|^2}$  (full expressions of  $\Theta$  for APT systems are in Appendix C). If we now define  $\alpha = V_2^+/V_1^+$ , we find that, for the system to function as a CPA,  $\alpha = \pm 1$  for the APT-symmetric circuits I and II consequently which is consistent with the above eigenvalue analysis. This means that to achieve CPA, the input at the two ports should have identical intensity and the same (or opposite) relative phase. However, the inductive-coupled PT case requires infinity  $\gamma$ , while the TL-coupled PT systems require  $\alpha = -i(\sqrt{2} + 1)$  (see Appendix B). These results clearly demonstrate that it is easier to implement CPA input conditions using APT rather than using PT systems.

To verify these results, we have practically built prototypes of two APT-CPAL systems. The gain contribution is realized by an active oscillator that has negative resistance established by a negative impedance converter (NIC). By delicately designing the values of all lumped elements of the NIC module, we are able to practically realize  $\eta \approx 1.02$  for two configurations. The experimentally measured eigenvalues are embedded in Fig. 2, and  $\Theta$  is also measured under different input conditions corresponding to the CPA and laser operation in Figs. 3(a) and 3(b), where the experimentally measured data are superimposed on simulation results. The blue and red lines are obtained for input conditions matching CPA and laser operation which is indeed confirmed by the small or large values of  $\Theta$  at  $\omega = 1$ .

### III. SENSITIVITY AND ROBUSTNESS OF APT-CPAL

Next, we analyze the impact of experimental imperfections, such as fabrication errors or experimental uncertainties, and the deviations of the system from its designed parameters. We expect deviations in the input condition for CPA due to its dependence on amplitude and phase relations between input ports, which are hard to maintain in the presence of uncertainties and imperfections. Below the lasing threshold, the scattering matrices for two types of APT-symmetric circuits and the TL-coupled PT-symmetric circuit are given by

$$\begin{aligned} S_I &= \frac{-2}{\eta^2 - 1} \begin{bmatrix} \frac{\eta^2 + 1}{2} & -\eta \\ -\eta & \frac{\eta^2 + 1}{2} \end{bmatrix}, \\ S_{II} &= \frac{2}{\eta^2 - 1} \begin{bmatrix} \frac{\eta^2 + 1}{2} & \eta \\ \eta & \frac{\eta^2 + 1}{2} \end{bmatrix}, \\ S_{TL} &= \frac{1}{\eta^2 - 1} \begin{bmatrix} 1 - \sqrt{2}\eta & -i\eta^2 \\ -i\eta^2 & 1 + \sqrt{2}\eta \end{bmatrix}. \end{aligned} \quad (4)$$

Here we scale  $\eta$  to  $\sqrt{2}\eta$  in  $S_{TL}$  such that in all cases the lasing threshold is  $\eta = 1$ . In the following, we will analyze the situation for the APT-symmetric type-I circuit, noting that the analysis for APT-symmetric type-II and TL-coupled PT-symmetric circuits is similar.

The eigenvalues of  $S_I$  and eigenvectors are

$$\lambda_{I\pm} = \left( \frac{\eta + 1}{\eta - 1} \right)^{\pm 1}, \quad |V_{I\pm}\rangle = (1, \mp 1)^T. \quad (5)$$

As  $\eta$  approaches 1,  $S_I$  and its eigenvalues can be approximated as

$$S_I = A \begin{bmatrix} 1 & -1 \\ -1 & 1 \end{bmatrix}, \quad \lambda_{I\pm} = (2A)^{\pm 1}, \quad (6)$$

where  $A = 2(\eta - 1)^{-1} \rightarrow \infty$ . When the CPA input condition  $|V_{I-}\rangle = (1, 1)^T$  experiences both amplitude deviation ( $v_1, v_2$ ) and phase deviation  $\Delta\phi$ , the input can be written as

$$\begin{aligned} |V_{in}\rangle &= (1 + v_1, (1 + v_2)e^{i\Delta\phi})^T \\ &\approx |V_{I-}\rangle + (v_1, v_2)^T + (0, i\Delta\phi)^T. \end{aligned} \quad (7)$$

The output is  $|V_{out}\rangle = S_I |V_{in}\rangle$  and its intensity is

$$\begin{aligned} \langle V_{out}|V_{out}\rangle &= \langle V_{in}|S_I^\dagger S_I|V_{in}\rangle \\ &= 8A_1^2(v_1^2 - 2v_1v_2 + v_2^2 + \Delta\phi^2). \end{aligned} \quad (8)$$

To simplify the dependence of output with the amplitude deviation strength, we assume  $v_{1,2}$  is in the range of  $[-\Delta V, \Delta V]$ , then the average output is

$$\begin{aligned} \overline{\langle V_{out}|V_{out}\rangle} &= 2A_1^2(\overline{v_1^2 - 2v_1v_2 + v_2^2} + \Delta\phi^2) \\ &= 8A_1^2\left(\frac{2}{3}\Delta V^2 + \Delta\phi^2\right). \end{aligned} \quad (9)$$

By normalizing with the input  $\langle V_{in}|V_{in}\rangle$  and replacing  $A_1$  with  $\lambda_{I+}$ , the value of  $\Theta$  is

$$\Theta_I = |\lambda_{I+}|^2 \left( \frac{\Delta V^2}{6} + \frac{\Delta\phi^2}{4} \right). \quad (10)$$

Similarly, for APT-symmetric type-II and TL-coupled PT-symmetric circuits, we derive

$$\Theta_{II} = |\lambda_{II+}|^2 \left( \frac{\Delta V^2}{6} + \frac{\Delta\phi^2}{4} \right), \quad (11)$$

and

$$\Theta_{TL} = |\lambda_{TL+}|^2 \left( \frac{\Delta V^2}{6 - 3\sqrt{2}} + \frac{\Delta\phi^2}{4} \right). \quad (12)$$

To compare these three systems, we need to make the minimum (CPA) and the maximum (amplifier,  $\Theta_{\max}$ ) of the  $\Theta$  identical to all systems, which requires all  $|\lambda_{+}|$  values be identical in Eqs. (10) to (12) since  $\Theta_{\max} = |\lambda_{+}|^2$ . This result shows that to make  $\Theta_{APT} = \Theta_{PT}$  when subject to the same phase deviation, the intensity deviation that APT systems can tolerate is 1.85 times larger than that of the PT system, indicating a better robustness. The above theoretical analysis is well verified by our numerical calculations shown in Figs. 4(a) and 4(b).

The device parameters' deviations can also shift the system away from the CPAL condition. Inspired by the sharp lineshape around the CPAL point and the better feasibility, we further explore the use of the APT-symmetric CPAL systems for sensing purposes. In two APT configurations, the positive feedback resistors of the NICs ( $R_1 = R$  in Appendix D) can be made from different transducers, such as pressure-sensitive and humidity-sensitive resistors illustrated in the inset of Fig. 4(c), to translate the variations of physical or chemical signals to resistive perturbations ( $\Delta R$ ). In this regard, let us assume that a subtle resistive perturbation  $\epsilon = \Delta R/R \ll 1$  is applied to two configurations. Such a tiny

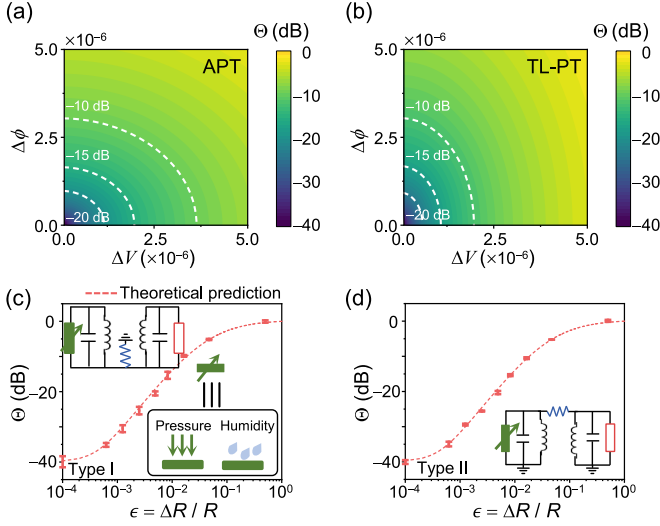


FIG. 4. (a), (b) demonstrate the contours of  $\Theta$  of two APT and transmission line (TL)-coupled PT systems, initially locked at their CPA, with respect to the tiny perturbations applied to excitation modes  $\Delta V$  and  $\Delta\phi$ . We note that two APT systems have the same robustness against such deviations, both stronger than the PT one. (c), (d) plot the sensitivity of two APT-CPAL sensors with respect to the resistive perturbations.

perturbation will shift the system away from the CPA operation state, demonstrating great sensitivity. To present the comparison in terms of sensitivity among two APT-CPAL and the PT-CPAL systems, we assume that each system initially operates at its CPA mode and has zero input deviation. Additionally, to avoid the infinite sensitivity when systems operate exactly at the CPAL point, we consider the practical scenario by introducing a fabrication error,  $\delta$ , into each structure. In two APT systems where ideally  $\eta_{\text{CPAL}} = 1$ , the fabrication error is introduced as  $\eta' = 1 + \delta$ . Similarly, in the TL-coupled PT system where ideal  $\eta_{\text{CPAL}} = 1/\sqrt{2}$ , the fabrication error makes  $\eta' = (1 + \delta)/\sqrt{2}$ . Then, a perturbation is applied to the feedback resistors of the NICs (assuming the gain element of PT systems is established by the NIC in the same form of APT),  $\epsilon = \Delta R/R \ll 1$ . Starting from the TL-coupled PT structure, we consider the most commonly employed structure in Appendix A, where a negative conductance and a positive conductance are separated by a quarter-wavelength transmission line that has an electrical length of  $\theta = \pi/2$ . The output factor as a function of the perturbation can be theoretically approximated as [27]

$$\Theta_{\text{TL}}(\epsilon) \approx \frac{1}{4} \left( \delta^2 + \frac{\epsilon^2}{\delta^2} \right) + O(\epsilon^3). \quad (13)$$

In the same vein, the output factor of both APT-CPAL sensors as functions of the same perturbation and fabrication error can be written as

$$\begin{aligned} \Theta_{\text{I}}(\epsilon) &= \frac{\delta^4 + \epsilon^2(1 + \delta)^2}{[\epsilon(1 + \delta) - \delta(2 + \delta)]^2} \\ &\approx \frac{1}{4} \left( \delta^2 + \frac{\epsilon^2}{\delta^2} \right) + O(\epsilon^3), \end{aligned}$$

$$\begin{aligned} \Theta_{\text{II}}(\epsilon) &= \frac{\delta^4 - 2\delta^4\epsilon + \epsilon^2[1 + \delta(2 + \delta + \delta^3)]}{[\epsilon - \delta(2 + \delta) + \delta(3 + \delta)\epsilon]^2} \\ &\approx \frac{1}{4} \left( \delta^2 + \frac{\epsilon^2}{\delta^2} \right) + O(\epsilon^3). \end{aligned} \quad (14)$$

The first term of these three approximations indicates the detection limit of the sensor while the second term denotes the sensitivity. Hence, we can make a conclusion that two types of APT-CPAL sensors can ideally have the same level of sensitivity as the PT-CPAL sensors when subject to the same amount of fabrication error, demonstrating that the robustness enhancement brought by our APT-CPAL systems do not sacrifice the response enhancement.

This is better demonstrated by plotting  $\Theta$  as a function of the perturbation as shown in Figs. 4(c) and 4(d), where the experimentally measured data points are embedded. As we can see, the response function data points experiences a change of over 40 dB over the perturbation range with strong sensitivity even for  $\epsilon \sim 10^{-4}$ . Further, we would like to highlight that due to the simplified circuit structures, two types of APT systems are more readily realizable in practice and the fabrication errors can be more precisely controlled which may help approach the maximum sensitivity of  $\sim 2500\epsilon^2$  predicted by theory and numerical simulations. This is a significant improvement over the sensitivity of  $\sim 4.5\epsilon^2$  reported in Ref. [28] for the TL-coupled PT sensor.

#### IV. CONCLUSION

In summary, we demonstrated a configuration of electronic APT systems, which, together with another one reported in Ref. [32], can have CPAL points when combined with an additional parity symmetry. These APT-symmetric circuits with parity symmetry can facilitate the implementation of a CPAL operation point with enhanced robustness regarding design, fabrication, and excitation compared to its PT counterparts, therefore exhibiting better practical sensitivity.

#### ACKNOWLEDGMENTS

Ş.K.Ö. and R.E. acknowledge support from the Air Force Office of Scientific Research (AFOSR) Multidisciplinary University Research Initiative (MURI) Award No. FA9550-21-1-0202.

#### APPENDIX A: HAMILTONIANS OF APT SYSTEMS

To make the circuit dynamics of the type I APT system more straightforward, we here introduce two resistors  $R_3$  and  $R_4$  as depicted in Fig. 5(a), which do not modify the scattering properties of the system. By applying Kirchoff's laws to type I APT schematic, we can simply write the circuit dynamics as

$$\begin{aligned} \frac{V_1}{L_1} + \frac{1}{R_3} \dot{V}_{10} + \frac{1}{R_1} \dot{V}_1 + C_1 \ddot{V}_1 &= 0, \\ \frac{V_2}{L_2} + \frac{1}{R_4} \dot{V}_{20} + \frac{1}{R_2} \dot{V}_2 + C_2 \ddot{V}_2 &= 0, \\ \frac{V_{10}}{R_3} + \frac{V_{20}}{R_4} + \frac{V_0}{R_c} &= 0, \end{aligned} \quad (A1)$$

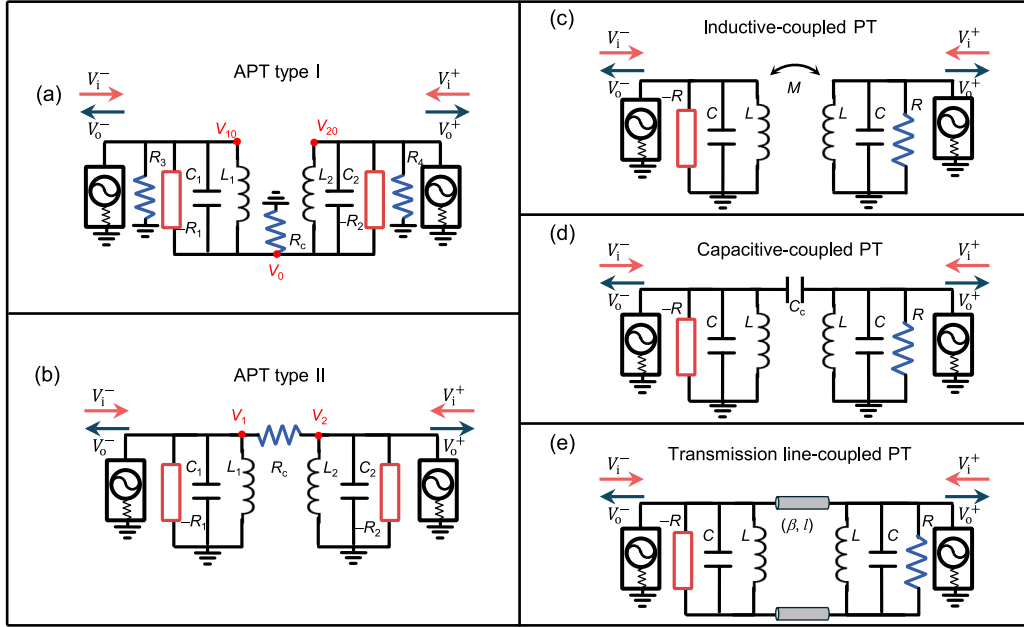


FIG. 5. (a), (b) are circuit diagrams of two APT systems. (c)–(e) present the circuit diagrams of inductive-, capacitive-, and transmission line (TL)-coupled PT systems.

where the dot denotes the time derivative,  $V_1 = V_{10} - V_0$ ,  $V_2 = V_{20} - V_0$ , and here  $V_{10}$ ,  $V_{20}$ , and  $V_0$  are the node voltages marked out by red dots in Fig. 5. By eliminating  $V_{10}$ ,  $V_{20}$ , and  $V_0$ , Eq. (A1) can be written as

$$\begin{aligned} \ddot{V}_1 + \omega_1^2 V_1 - \frac{1}{R_3 R_4 C_1 G} \dot{V}_2 + \left( \frac{1}{R_1 C_1} - \frac{R_4^{-1} + R_c^{-1}}{R_3 C_1 G} \right) \dot{V}_1 &= 0, \\ \ddot{V}_2 + \omega_2^2 V_2 - \frac{1}{R_3 R_4 C_2 G} \dot{V}_1 + \left( \frac{1}{R_2 C_2} - \frac{R_3^{-1} + R_c^{-1}}{R_4 C_2 G} \right) \dot{V}_2 &= 0, \end{aligned} \quad (\text{A2})$$

where  $G = R_3^{-1} + R_4^{-1} + R_c^{-1}$ .

This circuit dynamics can be recast to the Liouvillian formalism as

$$\begin{aligned} \frac{d\psi}{dt} = \mathcal{L}_I \psi, \quad \mathcal{L}_I &= \begin{bmatrix} 0 & 0 & 1 & 0 \\ 0 & 0 & 0 & 1 \\ -\omega_1^2 & 0 & g_1 & k_1 \\ 0 & -\omega_2^2 & k_2 & g_2 \end{bmatrix}, \\ g_1 = \frac{R_4^{-1} + R_c^{-1}}{R_3 C_1 G} - \frac{1}{R_1 C_1}, \quad g_2 = \frac{R_3^{-1} + R_c^{-1}}{R_4 C_2 G} - \frac{1}{R_2 C_2}, \\ k_1 = \frac{1}{R_3 R_4 C_1 G}, \quad k_2 = \frac{1}{R_3 R_4 C_2 G}, \end{aligned} \quad (\text{A3})$$

where  $\psi \equiv (V_1, V_2, \dot{V}_1, \dot{V}_2)$ . Alternatively, a  $2 \times 2$  Hamiltonian matrix of the type-I APT circuit can be obtained from the coupled-mode theory by adopting the slowly varying complex-envelope function as

$$V_n(t) = v_n(t) \exp(-i\omega_0 t) + v_n^*(t) \exp(i\omega_0 t), \quad (\text{A4})$$

here  $n = 1, 2$  denotes the nodes 1 and 2. Combined with an uncoupled resonance frequency  $\omega_0 = (\omega_1 + \omega_2)/2$ , the circuit dynamics can be approximated into a coupled-mode equation,

which yields the  $2 \times 2$  Hamiltonian to be

$$H_I = \begin{bmatrix} \Delta\omega + ig_1 & k_1 \\ k_2 & -\Delta\omega + ig_2 \end{bmatrix}, \quad (\text{A5})$$

where  $\Delta\omega = \omega_1 - \omega_2$ . Equation (A5) is the full expression of Eq. (1) in the main context. The APT symmetry condition, i.e.,  $\{PT, H\} = 0$  leads to  $C_1 = C_2 = C$  and  $R_1^{-1} - R_2^{-1} = (R_3^{-1} + R_c^{-1})/(R_4 G) - (R_4^{-1} + R_c^{-1})/(R_3 G)$ .

Similarly, the circuit dynamics of the type-II APT system shown in Fig. 5(b) can be expressed as

$$\begin{aligned} \ddot{V}_1 + \frac{1}{C_1} \left( \frac{1}{R_c} - \frac{1}{R_1} \right) \dot{V}_1 + \omega_1^2 V_1 - \frac{1}{R_c C_1} \dot{V}_2 &= 0, \\ \ddot{V}_2 + \frac{1}{C_2} \left( \frac{1}{R_c} - \frac{1}{R_2} \right) \dot{V}_2 + \omega_2^2 V_2 - \frac{1}{R_c C_2} \dot{V}_1 &= 0. \end{aligned} \quad (\text{A6})$$

The Liouvillian matrix can be expressed as

$$\begin{aligned} \mathcal{L}_{II} &= \begin{bmatrix} 0 & 0 & 1 & 0 \\ 0 & 0 & 0 & 1 \\ -\omega_1^2 & 0 & g_3 & k_3 \\ 0 & -\omega_2^2 & k_4 & g_4 \end{bmatrix}, \quad g_3 = \frac{R_1 - R_c}{R_1 C_1 R_c}, \\ g_4 = \frac{R_2 - R_c}{R_2 C_2 R_c}, \quad k_3 = \frac{1}{R_c C_1}, \quad k_4 = \frac{1}{R_c C_2}. \end{aligned} \quad (\text{A7})$$

However, the  $2 \times 2$  coupled-mode Hamiltonian matrix reads

$$H_{II} = \begin{bmatrix} \Delta\omega + ig_3 & ik_3 \\ ik_4 & -\Delta\omega + ig_4 \end{bmatrix}. \quad (\text{A8})$$

The APT condition requires  $R_1 = R_2$  and  $C_1 = C_2$  while the inductances are not necessarily the same. In Appendix B,

we theoretically prove that the CPAL condition additionally requires that  $L_1 = L_2$  for both types of APT circuits, which simplifies the two APT Hamiltonian matrices to

$$H_I = i \begin{bmatrix} g_1 & k_1 \\ k_1 & g_1 \end{bmatrix}, \quad H_{II} = i \begin{bmatrix} g_3 & k_3 \\ k_3 & g_3 \end{bmatrix}. \quad (\text{A9})$$

We can then easily verify that  $[P, H_{I,II}] = 0$ , satisfying the parity symmetry.

## APPENDIX B: SCATTERING MATRICES

### 1. S matrix of two kinds of APT-symmetric circuits

In this section, we provide the explicit expression of scattering matrices of two APT and three PT systems shown in Fig. 5 starting from the APT cases. For APT cases, we first assume that two systems have parity symmetry ( $-R_1 = -R_2$ ,  $C_1 = C_2$ , and  $L_1 = L_2$ , which will be proven to be necessary later). To derive the corresponding scattering matrices, we can analyze the systems using the transmission-line network (TLN) equivalence and write the admittance matrices of them by cascading the ABCD matrices of each electronic

component [36], which have the following form:

$$Y_I = \begin{bmatrix} y_1 & y_2 \\ y_2 & y_1 \end{bmatrix},$$

$$y_1 = -\frac{[i + (\gamma - i\omega)\omega]\{-\gamma\omega + \kappa[i + (\gamma - i\omega)\omega]\}}{\gamma\eta\omega\{-\gamma\omega + 2\kappa[i + (\gamma - i\omega)\omega]\}},$$

$$y_2 = \frac{\kappa[i + (\gamma - i\omega)\omega]^2}{\gamma\eta\omega\{-\gamma\omega + 2\kappa[i + (\gamma - i\omega)\omega]\}},$$

$$Y_{II} = \begin{bmatrix} \frac{\gamma\omega - \gamma\kappa\omega + i\kappa(\omega^2 - 1)}{\gamma\eta\kappa\omega} & -\frac{1}{\eta\kappa} \\ -\frac{1}{\eta\kappa} & \frac{\gamma\omega - \gamma\kappa\omega + i\kappa(\omega^2 - 1)}{\gamma\eta\kappa\omega} \end{bmatrix}, \quad (\text{B1})$$

where  $\gamma = R^{-1}(L/C)^{1/2}$  is the systems' quality factor,  $\kappa = M/L$  denotes the inductive coupling strength between two inductors where  $M$  ( $L$ ) is the mutual (self) inductance of the coil inductor, and  $\eta = R/Z_0$  and  $Z_0$  is the characteristic port impedance of the vector network analyzer (VNA). We should point out here that when measuring the scattering property,  $R_3$  and  $R_4$  are actually the port impedance. These two admittance matrices, being linearly transformed, can yield the scattering matrices accordingly, which can be written as

$$S_j = \begin{bmatrix} r_j & t_j \\ t_j & r_j \end{bmatrix}, \quad j = \text{I or II};$$

$$t_I = \frac{2\eta\kappa[\gamma\omega + i(1 - \omega^2)]^2}{[\gamma\omega(\eta - 1 - 2\eta\kappa) + i(1 + 2\eta\kappa)(\omega^2 - 1)][\gamma\omega(\eta - 1) + i(\omega^2 - 1)]},$$

$$r_I = \frac{1}{1 + 2\eta\kappa} \left[ -1 + \frac{\gamma\eta\omega}{\gamma\omega(\eta - 1 - 2\eta\kappa) + i(1 + 2\eta\kappa)(\omega^2 - 1)} + \frac{\gamma\eta\omega(1 + 2\eta\kappa)}{\gamma\omega(\eta - 1) + i(\omega^2 - 1)} \right],$$

$$t_{II} = \frac{2\eta\gamma^2\omega^2\kappa^{-1}}{[\gamma\omega(\eta - 1) + i(\omega^2 - 1)][\gamma\omega(\eta - 1 + 2\kappa^{-1}) + i(\omega^2 - 1)]},$$

$$r_{II} = -1 + \gamma\eta\omega \left[ \frac{1}{\gamma\omega(\eta - 1) + i(\omega^2 - 1)} + \frac{1}{\gamma\omega(\eta - 1 + 2\kappa^{-1}) + i(\omega^2 - 1)} \right]. \quad (\text{B2})$$

The CPAL effect of both APT configurations occurs at  $\kappa = \eta = \omega = 1$ . At  $\omega = 1$  and close to the CPAL point ( $\eta \rightarrow 1$ ), the scattering matrices of both systems can be simplified to

$$S_I = -A \begin{bmatrix} 1 & -1 \\ -1 & 1 \end{bmatrix}, \quad S_{II} = A \begin{bmatrix} 1 & 1 \\ 1 & 1 \end{bmatrix}, \quad (\text{B3})$$

where  $A = 2(\eta - 1)^{-1}$  approaches infinity.

Additionally, here we also theoretically demonstrate that the system must obey the parity symmetry to have the CPAL phenomenon ( $-R_1 = -R_2$ ,  $C_1 = C_2$ , and  $L_1 = L_2$ ). First, for

the type-I APT circuit shown in Fig. 5(a),  $R_3 = R_4$  is equivalent to the port impedance when measuring the scattering properties, which makes  $-R_1 = -R_2$  and  $C_1 = C_2$  already to satisfy the APT condition (see Appendix A). Therefore, we introduce a scaling factor  $L_1 = sL_2$  to the system to validate whether  $s = 1$  (parity symmetry) is mandatory for the type-I APT system to exhibit the CPAL effect. Following the same procedure, we can have a new and more complicated scattering matrix whose eigenvalues at  $\omega = 1$  yield

$$\lambda_{I\pm} = \frac{2[s(i - \gamma) - i]\eta\kappa \pm \sqrt{\{s\gamma[1 + \eta^2(2\kappa - 1)] - i(s - 1)[1 + \eta(\eta\kappa - 1)]\} \times \{i(1 + \eta + \eta^2\kappa) + s[\gamma + \gamma\eta^2(2\kappa - 1) - i(1 + \eta + \eta^2\kappa)]\}}}{-s[i + \gamma(\eta - 1)](\eta - 1) + s[2\gamma(\eta - 1) - i(\eta - 2)]\eta\kappa + i[\eta - 1 + (\eta - 2)\eta\kappa]}. \quad (\text{B4})$$

By solving  $\lambda_{I-} = 0$  and  $\lambda_{I+} = \infty$  (CPAL condition), we have the scaling factor,  $s_I$ , for the type-I APT circuit expressed as

$$s_I = \frac{(1 - \eta + 2\eta^2\kappa)^2 - i\gamma(1 - \eta + 2\eta^2\kappa)(\eta - 1)[1 + \eta(2\kappa - 1)]}{\gamma^2(1 - \eta)^2(1 - \eta + 2\eta\kappa)^2 - [1 - \eta - (\eta - 2)\eta\kappa]^2}. \quad (\text{B5})$$

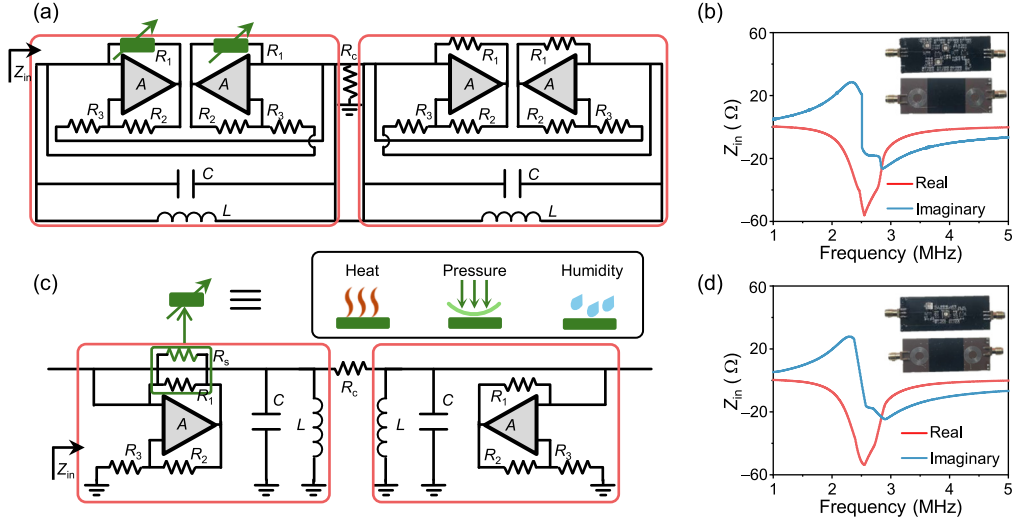


FIG. 6. (a), (b) are the detailed circuit schematic of the type I APT structure and the measured input impedance, respectively. (c), (d) are similar to (a), (b) but for the type-II APT structure. At the resonance frequency where  $\text{Im}(Z_{\text{in}}) = 0$ ,  $\text{Re}(Z_{\text{in}}) \approx -51 \Omega$ , yielding  $\eta \approx 1.02$ .

Since the scaling factor must be positive and purely real, we need to make the imaginary part of Eq. (B5) zero, leading to  $\eta = 1$ , which coincidentally is the lasing threshold of the CPAL point. This, in turn, makes  $s_1 = 1$ , strongly validates that the type-I APT system must additionally satisfy the parity symmetry to exhibit the CPAL phenomenon.

Similarly, the scaling factor  $s_{\text{II}}$ , for type-II APT circuit when the CPAL point is ensured reads

$$s_{\text{II}} = \frac{i[1 + (\eta - 1)\kappa]}{i[1 + (\eta - 1)\kappa] + \gamma(\eta - 1)[2 + (\eta - 1)\kappa]}. \quad (\text{B6})$$

Equation (B6), although different from Eq. (B5), provides the same result that when its imaginary part becomes zero,  $s_{\text{II}} = 1$ . Therefore, we can conclude that for both types of APT systems,  $L_1 = L_2$  is mandatory to have the CPAL point, which makes the Hamiltonian in Eqs. (A5) and (A8) additionally satisfy the parity symmetry.

## 2. S matrix of PT-symmetric circuits coupled through an inductor

By applying the same method used before, the complete scattering matrix for the PT-symmetric circuits based on mutual inductive coupling ( $S_L$ ) [Fig. 5(c)] is

$$S_L = \frac{1}{T} \begin{bmatrix} X_+ - 1 + 2\omega^2 & 2i\gamma\eta\mu\omega \\ 2i\gamma\eta\mu\omega & X_- - 1 + 2\omega^2 \end{bmatrix}, \quad (\text{B7})$$

where  $T = 1 + \omega\{\gamma^2(\eta^2 - 1)(\kappa^2 - 1)\omega + 2i\gamma\eta[1 + (\mu^2 - 1)\omega^2] - (\mu^2 - 1)\omega^3 - 2\omega\}$ ,  $X_{\pm} = \gamma^2[1 + \gamma^2(\eta \pm 1)^2(\mu^2 - 1)\omega^2 + (\mu^2 - 1)\omega^4]$  to simplify Eq. (B7),  $\mu = M/L$  is the inductive coupling strength. For the scattering matrix in Eq. (B7), the CPAL condition is  $\eta = 1$  and  $\gamma = \infty$ . In addition, the CPAL effect occurs at  $\omega = (1 - \mu^2)^{-1/2}$ . When the system is close to CPAL condition, the  $S_L$  can be written

as

$$S_L = B_1 \begin{bmatrix} \frac{i\mu}{\omega^2 + (\mu^2 - 1)\omega^4} & 1 \\ 1 & -(\frac{\mu}{\omega^2 + (\mu^2 - 1)\omega^4})^{-1} \end{bmatrix},$$

$$B_1 = \frac{i\mu\omega[2\omega^2 + (\mu^2 - 1)\omega^4 - 1]}{\omega + (\mu^2 - 1)\omega^3} \rightarrow \infty. \quad (\text{B8})$$

It is worth noting that the CPA excitation mode of this inductive-coupled PT schematic,  $\alpha = V_1^+/V_2^+ = -i\frac{2\gamma\mu\sqrt{1+\mu^2}}{\mu^2+4\gamma^2(\mu^2-1)}$  is purely imaginary and will approach zero for CPA condition since  $\gamma \rightarrow \infty$ , which corresponds to a single excitation. Since this inductive-coupled PT system requires an infinity  $\gamma$  to exhibit the CPAL effect which is physically impossible in reality, we do not put this case into our robustness and sensitivity comparisons.

## 3. S matrix of PT-symmetric circuits coupled through a capacitor

The situation for the PT-symmetric circuits coupled through a capacitor [Fig. 5(d)] is quite similar to the inductive coupling case. The complete scattering matrix ( $S_C$ ) reads

$$S_C = \frac{1}{Y_- + 2i\gamma\eta\omega Z - (2+c)\omega^2} \times \begin{bmatrix} (2+c)\omega^2 + Y_+ & 2i\gamma\eta\omega \\ 2i\gamma\eta\omega & (2+c)\omega^2 + Y_- \end{bmatrix}, \quad (\text{B9})$$

where  $Y_{\pm} = \gamma^2(\eta \pm 1)^2(\omega - 1)^2[(2+c)\omega^2 - \kappa]$  and  $Z = 1 + c - (2+c)\omega^2$  to simplify Eq. (B9); here,  $c = C_c/C$  is the capacitive coupling strength. The CPAL effect occurs only at  $\eta = 1$  and  $\gamma = \infty$ . Close to the CPAL point, Eq. (B9) can be simplified to  $S_C = B_2 \begin{bmatrix} Z^{-1} & 1 \\ 1 & Z \end{bmatrix}$ , where  $B_2 = \frac{(2+c)\omega^2}{1+c-(2+c)\omega^2} \rightarrow \infty$ . Thus, we find interestingly that the CPAL point similarly does not occur at  $\omega = 1$  in this scenario, but  $\omega = \sqrt{\frac{c+1}{c+2}}$  instead, which agrees with the observation in Ref. [19]. It is



also worth noting that achieving an infinite  $\gamma$  with finite  $\eta$  and  $\kappa$  in this electronic system is practically impossible. Hence, one can only approach but never exactly be at the CPAL in this capacitive-coupled PT system. At the same time, the CPA excitation mode is  $\alpha = -i\frac{\sqrt{6}\gamma}{3-2\gamma^2}$ , which goes to zero when approaching the CPAL condition ( $\gamma \rightarrow \infty$ ). This result also indicates a single-port excitation.

#### 4. S matrix of PT-symmetric circuits coupled via a TL

The scattering matrix for the PT-symmetric circuits coupled via a TL ( $S_{\text{TL}}$ ) [Fig. 5(e)] is

$$S_{\text{TL}} = \frac{1}{i(2\eta^2 - 1) + 2\eta^2 \cot(\theta)} \times \begin{bmatrix} i(1 - 2\eta) & 2\eta^2 \csc(\theta) \\ 2\eta^2 \csc(\theta) & i(1 + 2\eta) \end{bmatrix}, \quad (\text{B10})$$

where  $\theta = \beta l$ ,  $\beta$ , and  $l$  are the wave number and the physical length of the TL [27]. The CPAL condition occurs only at  $\theta = \pi/2$  and  $\eta = 1/\sqrt{2}$ . In the vicinity of CPAL point  $\eta \rightarrow 1/\sqrt{2}$ , the scattering matrix can be simplified

$$\begin{aligned} \Theta_{\text{I,CPA}} &= \frac{(1 - 2\eta\kappa)^2 + \{-2(1 - 2\eta\kappa)^2 + \gamma^2[(1 - 2\eta\kappa) + \eta]^2\}\omega^2 + (1 - 2\eta\kappa)^2\omega^4}{(1 + 2\eta\kappa)^2 + [\gamma^2(\eta - 1 + 2\eta\kappa)^2 - 2(1 + 2\eta\kappa)^2\omega^2 + (1 + 2\eta\kappa)^2\omega^4]}, \\ \Theta_{\text{II,CPA}} &= \frac{[-2\gamma\omega + \gamma(1 + \eta)\kappa\omega]^2 + \kappa(-1 + \omega^2)^2}{[2\gamma\omega + \gamma(-1 + \eta)\kappa\omega]^2 + \kappa(-1 + \omega^2)^2}. \end{aligned} \quad (\text{C1})$$

However, when input signals correspond to the lasing eigenvectors of the system where  $|V_{\text{I}+}\rangle = \frac{1}{\sqrt{2}}(1, -1)^T$  and  $|V_{\text{II}+}\rangle = \frac{1}{\sqrt{2}}(1, 1)^T$ , the output factors of both system may become infinitely large ( $\Theta \approx \infty$ ), in the ideal scenario. The output factors of both systems under lasing modes have the same form as

$$\Theta_{\text{I,Lasing}} = \Theta_{\text{II,Lasing}} = 1 + \frac{4\gamma^2\eta}{1 + \gamma^2(\eta - 1)^2 - (2 - \omega^2)\omega^2}. \quad (\text{C2})$$

These four equations govern the CPA-lasing behaviors of two APT structures in Fig. 3 in the main text.

#### APPENDIX D: EXPERIMENTAL SETUPS

To experimentally realize the APT symmetry in electronics, the gain contribution to the system is realized by an active oscillator that has negative resistance established by a negative impedance converter (NIC). The NIC exploited in this work is made from an operational amplifier (OPAMP; THS3201, Texas Instruments Inc.) with a positive feedback circuit topology. Specifically, for type-I APT structure, the

as  $S_{\text{TL}} = B_3 \begin{bmatrix} i(1 - \sqrt{2}) & 1 \\ 1 & i(1 + \sqrt{2}) \end{bmatrix}$ , where  $B_3 = i(2\eta^2 - 1)^{-1} \rightarrow \infty$ , which corresponds to the CPA excitation mode of this TL-coupled PT schematic, i.e.,  $\alpha = -i(\sqrt{2} + 1)$ .

Now, we can make a simple conclusion that from the observation of all five scattering matrices, we find that the excitation modes of two APT systems are the simplest, i.e.,  $\alpha = \pm 1$ . Compared to their PT counterparts with purely imaginary values of  $\alpha$ , it is natural to say that achieving the APT-enabled CPAL effect is much more feasible in practice.

#### APPENDIX C: NORMALIZED OUTPUT ENERGIES OF APT-CPAL

The normalized output energy of a two-port network is defined in the main context as  $\Theta = \frac{|V_{\text{I}^-}|^2 + |V_{\text{II}^-}|^2}{|V_{\text{I}^+}|^2 + |V_{\text{II}^+}|^2}$ , which corresponds to the ratio between total output power to total input power of the system. When the systems are excited by the CPA mode, i.e.,  $|V_{\text{I}^-}\rangle = \frac{1}{\sqrt{2}}(1, 1)^T$  and  $|V_{\text{II}^-}\rangle = \frac{1}{\sqrt{2}}(1, -1)^T$ , their output factors may approach zero ( $\Theta \approx 0$ ). The expressions of both APT systems operating at CPA mode simply read

floating negative resistance is realized by a cross-coupled pair of two NICs, shown in Fig. 6(a). The resistors of each NIC are delicately selected to be  $R_2 = R_3 = 360 \Omega$ , and a potential trimmer in the range of  $R_1 = 0-100 \Omega$  to realize the desired value of negative resistance; here, the resistors in each NIC section are kept the same to balance the negative resistances in both oscillators. Combined with the voltage-controlled varactors and planar coil inductors, two oscillators can be precisely controlled to be identical, satisfying the parity symmetry, which we plot in Fig. 6(b). In particular, the measured negative resistance is sufficiently precise in the very vicinity of the designed frequency to support the APT-CPAL effect since it is monochromatic.

Similar to the floating scenario, the type-II APT-symmetric circuit can be more readily constructed by a single grounded NIC with fewer parasitics, as depicted in Fig. 6(c). The measured input impedance of this active oscillation tank is shown in Fig. 6(d). For both APT configurations, the input impedance is tailored to be  $Z_{\text{in}} \approx -51 \Omega$  close to the CPAL frequency, yielding  $\eta \approx 1.02$ .

It is worth noting that the measured output coefficients have slight discrepancies from the simulation results in Fig. 3 in the main context. To better explain this, we take the type II circuit as an example, which we plot a more practical circuit

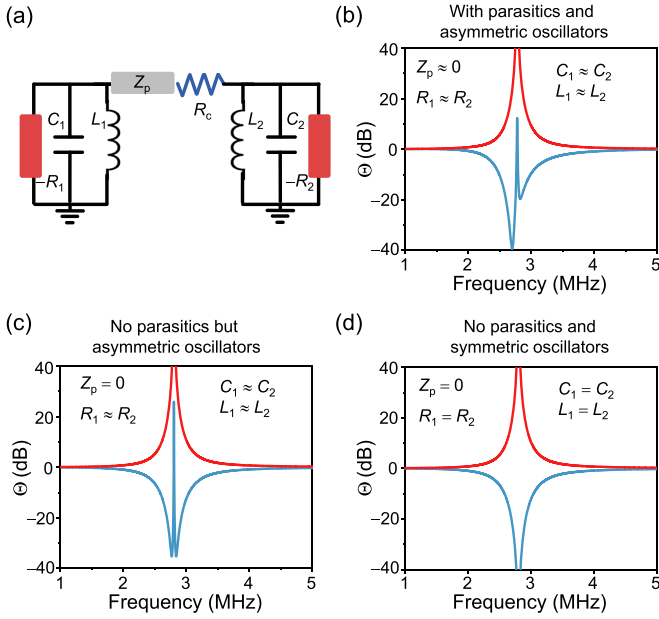


FIG. 7. (a) The type-II APT circuit schematic in a more practical consideration where  $Z_p$  represents the summarized parasitics of the system and each lumped element in two oscillators is slightly different. (b) The simulated  $\Theta$  when there exist parasitics and asymmetry between two oscillators, which shows a small frequency detuning between CPA and lasing points and a sharp peak on the CPA line. (c) The simulated  $\Theta$  when the parasitics are removed, where the frequency detuning disappears with only the sharp peak remaining the same. (d) The simulated  $\Theta$  when the simulation setup perfectly satisfies the APT symmetry ( $Z_p = 0$  and all lumped elements are identical in two oscillators) where the lineshape also becomes perfect.

structure in Fig. 7(a). The values of lumped elements of two  $-RLC$  oscillators are denoted by  $-R_{1(2)}$ ,  $C_{1(2)}$ , and  $L_{1(2)}$ , and the parasitic effect of the entire circuit (e.g., the nonlinear effect from the NIC module) is summarized as an impedance  $Z_p$ . By setting  $Z_p \neq 0$ ,  $-R_1 \approx -R_2$ ,  $C_1 \approx C_2$ , and  $L_1 \approx L_2$  in the circuit simulator (Advanced Design System) to mimic the realistic scenarios, the simulation results of output coefficients for CPA operation, as shown in Fig. 7(b), exhibit a significant frequency detuning compared to the lasing operation with an additional sharp peak. Then, when we remove the parasitics by setting  $Z_p = 0$ , the frequency mismatch between the CPA and lasing points disappears, as plotted in Fig. 7(c). Finally, under the perfect scenario that all the values of lumped elements in two oscillators are identical, the sharp peak that occurred to the CPA line is eliminated, rendering a perfect CPAL point of the system. In our experiment, we use a high-performance OPAMP, a voltage-controlled varactor, and a planar coil to precisely control the parasitic effect and balance the operation of two oscillators, which, although not extremely perfect, leads to a very slight difference between the measurements and simulations in Fig. 3 in the main text.

Additionally, to evaluate the sensing performances of both APT-CPAL configurations, the perturbations ( $\Delta R$ ) are applied to the feedback resistors of only one oscillation tank by paralleling a large resistor, as exemplified in Fig. 6(c). By doing so, the equivalent negative resistance of the NIC will become  $-R_{\text{NIC}} = -(R_1 // R_s)$  (the symbol “//” denotes the parallel connection). For example,  $-R_{\text{NIC}} = -R_1 = -51 \Omega$  without paralleling the large resistor to make the system operate at the CPAL point. When  $R_s = 5 \text{ M}\Omega$ ,  $-R_{\text{NIC}} = -(51 // 5 \times 10^6 \Omega) = -50.984 \Omega$ , leading to  $\Delta R = 0.052 \Omega$  and  $\epsilon = \Delta R / R_1 = 0.001$ .

- [1] C. M. Bender and S. Boettcher, Real spectra in non-Hermitian Hamiltonians having  $PT$  symmetry, *Phys. Rev. Lett.* **80**, 5243 (1998).
- [2] C. M. Bender, S. Boettcher, and P. N. Meisinger,  $PT$ -symmetric quantum mechanics, *J. Math. Phys.* **40**, 2201 (1999).
- [3] L. Feng, R. El-Ganainy, and L. Ge, Non-Hermitian photonics based on parity–time symmetry, *Nat. Photon.* **11**, 752 (2017).
- [4] R. El-Ganainy, K. G. Makris, M. Khajavikhan, Z. H. Musslimani, S. Rotter, and D. N. Christodoulides, Non-Hermitian physics and  $PT$  symmetry, *Nat. Phys.* **14**, 11 (2018).
- [5] Ş. K. Özdemir, S. Rotter, F. Nori, and L. Yang, Parity–time symmetry and exceptional points in photonics, *Nat. Mater.* **18**, 783 (2019).
- [6] R. El-Ganainy, M. Khajavikhan, D. N. Christodoulides, and Ş. K. Özdemir, The dawn of non-Hermitian optics, *Commun. Phys.* **2**, 37 (2019).
- [7] M.-A. Miri and A. Alù, Exceptional points in optics and photonics, *Science* **363**, eaar7709 (2019).
- [8] A. Krasnok, D. Baranov, H. Li, M.-A. Miri, F. Monticone, and A. Alù, Anomalies in light scattering, *Adv. Opt. Photonics* **11**, 892 (2019).
- [9] Y. D. Chong, L. Ge, H. Cao, and A. D. Stone, Coherent perfect absorbers: Time-reversed lasers, *Phys. Rev. Lett.* **105**, 053901 (2010).
- [10] Y. Slobodkin, G. Weinberg, H. Hörner, K. Pichler, S. Rotter, and O. Katz, Massively degenerate coherent perfect absorber for arbitrary wavefronts, *Science* **377**, 995 (2022).
- [11] H. Noh, Y. Chong, A. D. Stone, and H. Cao, Perfect coupling of light to surface plasmons by coherent absorption, *Phys. Rev. Lett.* **108**, 186805 (2012).
- [12] Y. D. Chong and A. D. Stone, Hidden black: Coherent enhancement of absorption in strongly scattering media, *Phys. Rev. Lett.* **107**, 163901 (2011).
- [13] W. R. Sweeney, C. W. Hsu, S. Rotter, and A. D. Stone, Perfectly absorbing exceptional points and chiral absorbers, *Phys. Rev. Lett.* **122**, 093901 (2019).
- [14] Q. Zhong, S. Nelson, Ş. K. Özdemir, and R. El-Ganainy, Controlling directional absorption with chiral exceptional surfaces, *Opt. Lett.* **44**, 5242 (2019).
- [15] C. Wang, W. R. Sweeney, A. D. Stone, and L. Yang, Coherent perfect absorption at an exceptional point, *Science* **373**, 1261 (2021).
- [16] S. Soleymani, Q. Zhong, M. Mokim, S. Rotter, R. El-Ganainy, and Ş. K. Özdemir, Chiral and degenerate perfect

- absorption on exceptional surfaces, *Nat. Commun.* **13**, 599 (2022).
- [17] S. Longhi,  $\mathcal{PT}$ -symmetric laser absorber, *Phys. Rev. A* **82**, 031801(R) (2010).
- [18] Z. J. Wong, Y.-L. Xu, J. Kim, K. O'Brien, Y. Wang, L. Feng, and X. Zhang, Lasing and anti-lasing in a single cavity, *Nat. Photon.* **10**, 796 (2016).
- [19] J. Schindler, Z. Lin, J. Lee, H. Ramezani, F. M. Ellis, and T. Kottos,  $\mathcal{PT}$ -symmetric electronics, *J. Phys. A: Math. Theor.* **45**, 444029 (2012).
- [20] Z. Lin, J. Schindler, F. M. Ellis, and T. Kottos, Experimental observation of the dual behavior of  $\mathcal{PT}$ -symmetric scattering, *Phys. Rev. A* **85**, 050101(R) (2012).
- [21] X. Zhu, H. Ramezani, C. Shi, J. Zhu, and X. Zhang,  $\mathcal{PT}$ -symmetric acoustics, *Phys. Rev. X* **4**, 031042 (2014).
- [22] P.-Y. Chen, M. Sakhdari, M. Hajizadegan, Q. Cui, M. M.-C. Cheng, R. El-Ganainy, and A. Alù, Generalized parity–time symmetry condition for enhanced sensor telemetry, *Nat. Electron.* **1**, 297 (2018).
- [23] M. Sakhdari, M. Hajizadegan, Q. Zhong, D. N. Christodoulides, R. El-Ganainy, and P.-Y. Chen, Experimental observation of  $\mathcal{PT}$  symmetry breaking near divergent exceptional points, *Phys. Rev. Lett.* **123**, 193901 (2019).
- [24] Z. Xiao, H. Li, T. Kottos, and A. Alù, Enhanced sensing and nondegraded thermal noise performance based on  $\mathcal{PT}$ -symmetric electronic circuits with a sixth-order exceptional point, *Phys. Rev. Lett.* **123**, 213901 (2019).
- [25] R. Kononchuk, J. Cai, F. Ellis, R. Thevamaran, and T. Kottos, Exceptional-point-based accelerometers with enhanced signal-to-noise ratio, *Nature (London)* **607**, 697 (2022).
- [26] M. Yang, L. Zhu, Q. Zhong, R. El-Ganainy, and P.-Y. Chen, Spectral sensitivity near exceptional points as a resource for hardware encryption, *Nat. Commun.* **14**, 1145 (2023).
- [27] M. Farhat, M. Yang, Z. Ye, and P.-Y. Chen,  $\mathcal{PT}$ -symmetric absorber-laser enables electromagnetic sensors with unprecedented sensitivity, *ACS Photonics* **7**, 2080 (2020).
- [28] M. Yang, Z. Ye, M. Farhat, and P.-Y. Chen, Enhanced radio-frequency sensors based on a self-dual emitter-absorber, *Phys. Rev. Appl.* **15**, 014026 (2021).
- [29] M. Yang, Z. Ye, H. Pan, M. Farhat, A. E. Cetin, and P.-Y. Chen, Electromagnetically unclonable functions generated by non-Hermitian absorber-emitter, *Sci. Adv.* **9**, eadg7481 (2023).
- [30] L. Ge and H. E. Türeci, Antisymmetric  $\mathcal{PT}$ -photonic structures with balanced positive-and negative-index materials, *Phys. Rev. A* **88**, 053810 (2013).
- [31] P. Peng, W. Cao, C. Shen, W. Qu, J. Wen, L. Jiang, and Y. Xiao, Anti-parity–time symmetry with flying atoms, *Nat. Phys.* **12**, 1139 (2016).
- [32] Y. Choi, C. Hahn, J. W. Yoon, and S. H. Song, Observation of an anti- $\mathcal{PT}$ -symmetric exceptional point and energy-difference conserving dynamics in electrical circuit resonators, *Nat. Commun.* **9**, 2182 (2018).
- [33] H. Zhang, R. Huang, S.-D. Zhang, Y. Li, C.-W. Qiu, F. Nori, and H. Jing, Breaking anti- $\mathcal{PT}$  symmetry by spinning a resonator, *Nano Lett.* **20**, 7594 (2020).
- [34] D. Mukhopadhyay, J. M.P. Nair, and G. S. Agarwal, Anti- $\mathcal{PT}$  symmetry enhanced interconversion between microwave and optical fields, *Phys. Rev. B* **105**, 064405 (2022).
- [35] H. A. Haus, *Waves and Fields in Optoelectronics* (Prentice Hall, New York, 1984).
- [36] D. M. Pozar, *Microwave Engineering* (John Wiley & Sons, New York, 2011).